BILINGUAL PUBLISHING CO.
Pioneer of Global Academics Since 1984

Semiconductor Science and Information Devices
https://ojs.bilpublishing.com/index.php/ssid

ARTICLE

The Anneal Temperature Effect on the BTO and NZFO Films and Their Capacitance - Inductance Integrated Device

Zhen Zheng Yuhao Shi Chengjie Shi Chunqing Wang*

Dept. Electronics Packaging Technology, School of Materials Science and Engineering, Harbin Institute of Technology, Harbin, 150001, China

ARTICLE INFO

Article history
Received: 8 March 2019
Accepted: 15 April 2019
Published Online: 30 October 2019

Keywords:
Capacitor-inductor
Integrated device
BTO film
NZFO film
Anneal temperature

ABSTRACT

In this paper, a novel capacitor-inductor integrated structure was proposed. The dielectric material BaTiO3 (BTO) and ferromagnetic material Ni0.5Zn0.5Fe2O4 (NZFO) was prepared by sol-gel method. Phase composition and morphology of the thin films were characterized by XRD, SEM and AFM. The effect of annealing temperature on film crystallinity, surface morphology, dielectric properties and ferromagnetism was investigated. When the annealing temperature was 700 °C, the BTO film and the NZFO film got the better dielectric properties and ferromagnetic properties. Then the BTO thin film was spin-coated on the substrate, and the NZFO thin film was in-situ sintered on the BTO thin film. The composite film possessed both ferromagnetism and dielectric properties. Finally, an inductive coil was fabricated on the BTO/NZFO composite film to produce a capacitance and inductance integrated device.

1. Introduction

In an electronic system, the components with different functions can be classified into active devices and passive devices according to electrical conditions. Active devices can be integrated in a large scale by semiconductor processes. In contrast, passive devices are difficult to manufacture by semiconductor processes due to their complex structure [1]. Not only it increases the manufacturing cost of passive components, but also the management and installation costs of the electronic products occupy an increasing proportion. The integration of passive components has become a bottleneck restricting the integration of electronic systems and miniaturization of electronic products. Effective development of integrated passive devices (IPD) technology is a vital development direction in electronic packaging field [2]. Among them, the passive device integration technology based on microelectronics technology has become a promising technology due to its low cost, high precision, high reliability, environmental protection and energy saving. Importantly, this technology is well compatible with available semiconductor processes [3]. Based on this technology, passive components such as capacitors, inductors, and resistors can also be fabricated and integrated in electronic systems by semiconductor processes. In passive devices, thin film capacitors and thin film inductors are the research hotspot. The key to develop the thin film capacitors

**Corresponding Author:*
Chunqing Wang,
Dept. Electronics Packaging Technology, School of Materials Science and Engineering, Harbin Institute of Technology, Harbin, 150001, China;
Email: wangcq@hit.edu.cn

 DOI: https://doi.org/10.30564/ssid.v1i1.606

and thin film inductors is to prepare high-performace dielectric thin films and ferromagnetic thin film materials.

Barium titanate ($BaTiO_3$, BTO) has received extensive attention as a dielectric thin film material [4-6]. BTO is a lead-free ceramic material with excellent electrical property. Due to its excellent pyroelectric and electrothermal properties, BTO is considered as an ideal material for the film capacitors preparation [7-10]. The sol-gel method is a kind of low cost and easy operation method for preparing ceramic films. BTO films were prepared by this method.[11]. Ashiri [12] prepared a only 26 mm BTO film by sol-gel method. Li [13] prepared a BTO film by sol-gel method and achieved the stripping. Whittam [14] and others studied the effect of porosity on the properties of the film. It was found that the dielectric constant of $BaTiO_3$ could be increased by reducing the porosity. Tripkovic [15] and others successfully prepared BTO inks. The BTO was then patterned using inkjet printing. Suematsu [16] prepared a BTO nanocomposite ink, which was fabricated by spin coating ink on a wafer. Shin [17] used the sol-gel method to prepare BTO nano-arrays and they successfully fabricated piezoelectric nano-generators using the BTO piezoelectric property.

The magnetic material of the thin film inductor is NiZn ferrite ($Ni_{0.5}Zn_{0.5}Fe_2O_4$, NZFO). NZFO is a soft magnetic material with spinel structure, which has high resistivity, low eddy current loss, high Curie temperature, low temperature coefficient, high frequency performance and other advantages. It is applicable to prepare a variety of inductors, choking coils, filter coils, mid-cycle transformers, etc [18-20]. Gao [20], Liu [21], Zhong [22] and others used a sputtering method to prepare a NiZn ferrite film. The magnetic properties of the film were adjusted by adjusting the Zn content, the Ar gas pressure, and the sputtering angle. Hashi [23], Lee [24] and others used the electrophoretic deposition method to prepare ferrite film, and obtained a ferrite film with superior performance. Lezhong [25], Gao [26], Yusuf [27] and others used a sol-gel method to prepare a NiZn ferrite film, and controlled the saturation magnetization and coercive force of the ferrite film by doping modification and changing the annealing temperature.

In this paper, BTO and NZFO films were prepared by sol-gel method. We found that the degree of crystallization of the film made an important effect on the properties of the film, and the degree of crystallization was closely related to the annealing temperature. Therefore, the different annealing temperatures were set to study the effect on the phase, morphology and properties of the film. On this basis, the two thin film materials were composted to prepare a composite functional material film with both dielectric and magnetic properties. A novel capacitor-inductor integrated structure was proposed. By making conductive coils on the composite film, a capacitance and inductance integrated device was successfully fabricated.

2. Experiment

The BTO film and NZFO film in this work were synthesized using a sol–gel spin-coating method. The films were made onto a $Pt/Ti/SiO_2/Si(100)$ substrate and its dimension was 10 mm × 10 mm × 0.5 mm. The chemicals used in this study were barium acetate, tetrabutyl titanate, nickel acetate, zinc acetate, ferric nitrate, 2-methoxyethanol, acetic acid, acetylacetone, polyethylene glycol 400 (PEG400) and absolute ethyl alcohol, and they were all analytical grade reagents. The BTO sol-gel solution was prepared using barium acetate and tetrabutyl titanate as starting materials. The concentration of sol-gel solution was 0.3 M by using 2-methoxyethanol and acetic acid as solvents, acetylacetone as a chelating agent, PEG400 as a filmogen. Analogously, the NZFO sol-gel solution was prepared using nickel acetate, zinc acetate, ferric nitrate, 2-methoxyethanol, acetic acid and PEG400. and the concentration of this solution was 0.2 M. The final sol-gel solutions of BTO and NZFO was obtained after sufficient stirring, and then stood at room temperature for several days. Then the BTO and NZFO sol-gels were spin-coated onto a substrate, and subsequently dried at 300 ℃ to form the dry gel film., respectively. Finally, the dry gel films were annealed at a high temperature to form the crystallized film. The above process has been reported by our group [28].

The BTO film was firstly fabricated onto a substrate after annealing. Then, the NZFO film was fabricated onto the BTO film to get the BTO/NZFO composite film. The inductance coil was finally set onto the composite film. The capacitance and inductance integrated device was accomplished.

The phase compositions of the thin films were verified by X-ray diffraction (XRD) on a Philips X'Pert diffractometer with Cu Kα radiation. The scanning electron microscopy (SEM) images were investigated with an FEI Helios NanoLab 600i instrument. The atomic force microscopy (AFM) was carried out by a Bruker Dimension Icon system. The dielectric constant of the thin film was measured by an Agilent E4980A precision impedance analyzer. The magnetic hysteresis loops were examined by a vibrating sample magnetometer (VSM, Lake Shore 7410).

DOI: https://doi.org/10.30564/ssid.v1i1.606

3. Result and Discussion

3.1 Phase Compositions of the BTO Thin Films

The phase compositions of the BTO thin films with different annealing temperature were analyzed by the XRD, and the results were shown in Figure 1. As shown in the figure, the peaks of BTO thin films were in accordance with the PDF#74-1957 and there was no impurity phase appearing in the XRD pattern of the BTO thin films except the characteristic diffraction peaks of Pt. As the annealing temperature increased, it was found that the specific diffraction peaks intensities of the BTO crystals on the three crystal faces of (100), (110), and (200) gradually increased. It was indicated that the crystallization degree of the BTO films increased as the annealing temperature increased.

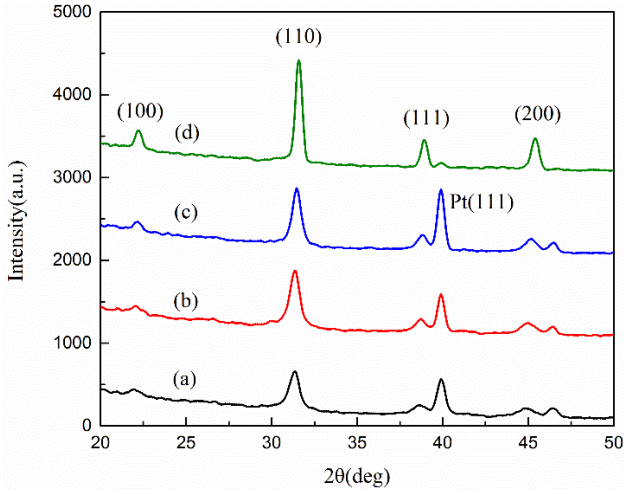

Figure 1. XRD patterns of the BTO thin films (a) 600℃ (b) 700℃ (c) 800℃ (d) 900℃

3.2 The Surface Morphology of BTO Thin Films

The SEM images from Figure 2 (a) - (d) were the surface morphologies of BTO thin films annealed at different temperatures. The BTO thin films were characterized a dense and fine-grained structure. According to the SEM images, the grain sizes of the BTO thin films were compared. At the annealing temperature of 600 °C, the degree of crystallization was poor, the crystal grains were very fine and the grain size was about 20 nm. When the annealing temperature increased to 700 °C, the grain size of the film had increased significantly, probably 50 to 100 nm. The grains began to merge with each other and the grain size became irregular at the annealing temperature of 800 °C. When the annealing temperature was increased to 900 °C, not only the sample grains merged with each other, but also some small crystal grains appeared on the large crystal grain boundaries, which would affect the film surface roughness . The AFM results were consistent with the SEM analysis. From the AFM images (a) - (d), the film samples roughness was below 20 nm at the annealing temperature from 600 ℃ to 800 ℃ . But it was increased significantly when the annealing temperature reached 900 °C. It could be attributed that the annealing time was too long and the crystal grains got excessively grown.

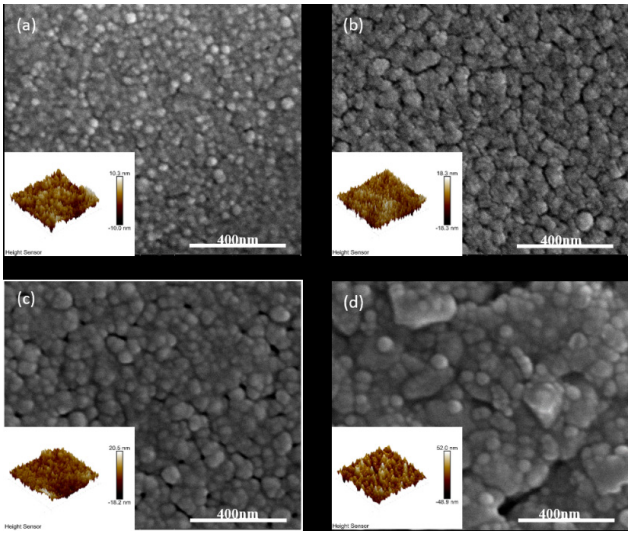

Figure 2. SEM images and AFM images of the BTO thin films (a) 600℃ (b) 700℃ (c) 800℃ (d) 900℃

3.3 The Dielectric Properties of the BTO Thin Films

The dielectric properties of the films with different annealing temperature were illustrated in Figure 3. The dielectric constants of film samples with different annealing temperatures were comparatively studied (1 kHz to 1 MHz). The dielectric constant of the film sample with 700°C annealing was substantially stable. Because the sample surface at 700°C was uniform and compact. Compared with the other sample dielectric constants, the dielectric constant was the largest, it was about 45. The sample dielectric constant at 800 °C was slightly lower than that of the sample at 700 °C, it was about 35. This change in dielectric constant could be ascribed to the different surface morphologies with the increased annealing temperature. The 600 °C annealing sample got the minimum dielectric constant of about 20 due to the poor degree of crystallization. When the annealing temperature reached 900 °C, some pores were observed on the sample surface, which decreasd the dielectric constant obviously, it was only about 25. From the above, 700 °C was selected as the annealing temperature.

 DOI: https://doi.org/10.30564/ssid.v1i1.606

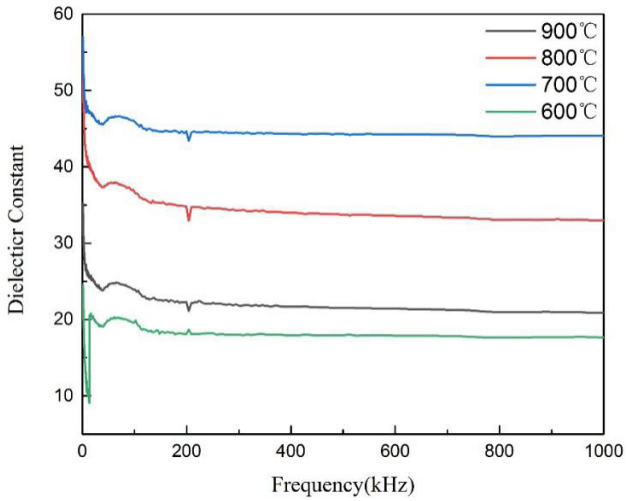

Figure 3. The dielectric constant of the BTO thin films at different frequencies

3.4 Phase Compositions of the NZFO Thin Films

The phase compositions of the NZFO thin films with different annealing temperature were analyzed by the XRD, and the results were shown in Figure 4. As shown in the figure, the peaks of NZFO thin films were in accordance with the PDF#52-278 and there was no impurity phase appearing in the XRD pattern of the NZFO thin films except the characteristic diffraction peaks of Pt. It was found that as the heat treatment temperature increased, the two characteristic diffraction peaks of (220) and (311) of NiZn ferrite gradually increased, which indicated that the degree of crystallization of NiZn ferrite was gradually increasing. In addition to the gradual increase of the characteristic diffraction peaks, the two characteristic peaks of (220) and (311) were gradually becoming narrower and narrower, which indicated that the grains of NiZn ferrite was gradually increasing.

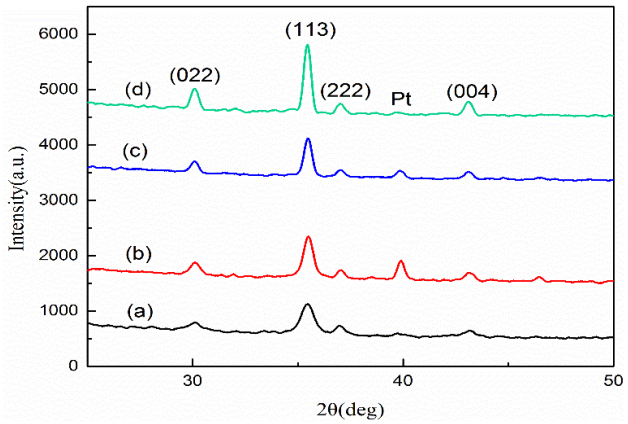

Figure 4. XRD patterns of the BTO thin films (a) 600℃ (b) 700℃ (c) 800℃ (d) 900℃

3.5 The Surface Morphology of BTO Thin Films

The SEM images from Figure5 (a) - (d) were the surface morphologies of BTO thin films annealed at different temperatures. From the above images, it was found that grains could be obviously seen in samples at 700 °C, 800 °C, and 900 °C, but it was difficult to see the grains in the sample at 600 °C, which confirmed the XRD characterization result that the crystallinity of the sample at 600 °C was the worst. As shown in above figures, it was found that the grains of the sample at 700 °C could be clearly seen, whose size was about 30 - 40 nm, and the film density was very high and few pores could be seen. When the annealing temperature rising to 800 °C, the size of the crystal grains increased and the size was about 100 nm, but microscopic pores began to appear. As the annealing temperature going to 900 °C, the grain size further increased to 200 nm. The roughness of the thin films was measured by the AFM. As shown in the AFM images, it could be seen that the surface of the sample at 600 °C and 700 °C was very flat. The surface roughness of the sample at 600 °C was only ± 2 nm, and the roughness of the sample at 700 °C was only ± 6 nm. At 800 °C, the roughness started to significantly increase to ±20 nm, and the roughness reached ± 35 nm at 900 °C. The roughness changes confirmed the conclusion drawn from the SEM that the growth of the grain caused the increase in roughness.

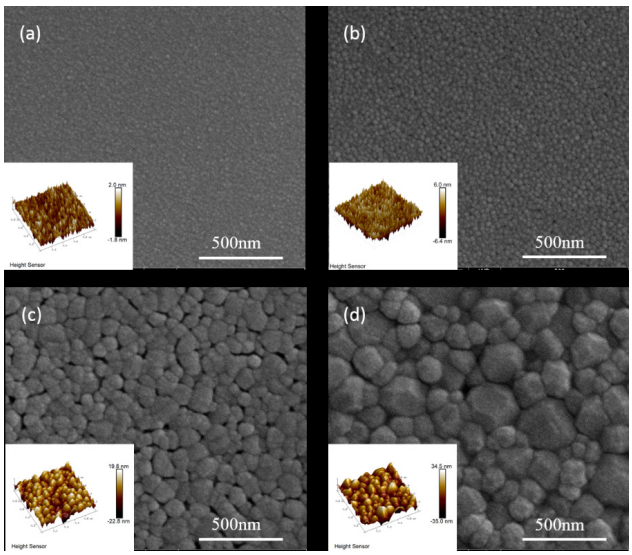

Figure 5. SEM images and AFM images of the NZFO thin films (a) 600℃ (b) 700℃ (c) 800℃ (d) 900℃

3.6 The Magnetic Properties of the BTO Thin Films

The magnetic hysteresis loops of the NZFO thin films with different temperature annealing were shown in Figure 6

DOI: https://doi.org/10.30564/ssid.v1i1.606

(a). It could be seen that the saturation magnetization of samples at 600 °C, 700 °C, and 800 °C was similar. The saturation magnetization of the sample at 900 °C was significantly higher than that of other samples. The reason was that the sample got the highest crystallinity at 900 °C, so its saturation magnetization was the highest. Figure 6 (b) showed the relationship between the saturation magnetization and the coercive force of annealing temperature. It was found that the saturation magnetization increased as the annealing temperature increasing, which proved that the saturation magnetization was positively correlated with the crystallinity of the sample. From 600 °C to 800 °C. It could be understood that as the annealing temperature increasing, the crystal grains became larger and the magnetic domains became larger. So the coercive force became bigger. With the combination of saturation magnetization, coercive force, film surface morphology and other factors, 700 °C was an ideal annealing temperature.

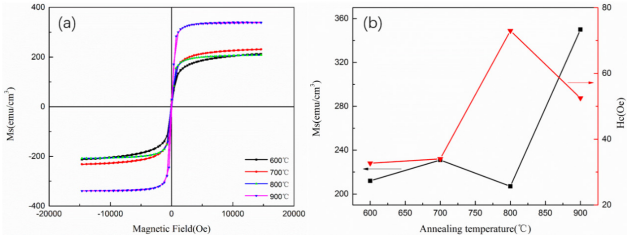

Figure 6 (a). The magnetic hysteresis loops of the NZFO thin films; (b). The saturation magnetization and coercive force of the NZFO thin films

3.7 The Capacitance and Inductance Integrated Device

The manufacturing process of the capacitance and inductance integrated device was shown in Figure 7 (a). Pt/Ti/SiO_2/Si multilayer was chosen as the substrate. First, the BTO sol was spin-coated onto the substrate and subsequently annealed at 700 ℃ to manufacture the BTO thin film. The NZFO sol was deposited onto the BTO using the same spin-coating process, followed by annealing at 700 ℃ . The cross-section drawn of the composite thin film was shown in Figure 7 (b). It could be clearly seen that there was a clear interface between the two films, which indicated that no composition diffusion happened between the two films. The composite film combined dielectric and ferromagnetic properties to enhance both capacitance and inductance of the device. Then, hydrofluoric acid was used to etch a corner of the composite film to expose the metal layer as the bottom electrode. A planar inductor without composite film was tested an inductance of 550 nH. The device was shown in Figure 7 (c) and the equivalent circuit of the device was shown in Figure 7 (d). The planar inductor was placed on the composite film and the inductance was measured to be 660 nH, was increased by 20 %. And A planar inductor without composite film was 30 pF, which exhibited that the device had both capacitive and inductive functions.

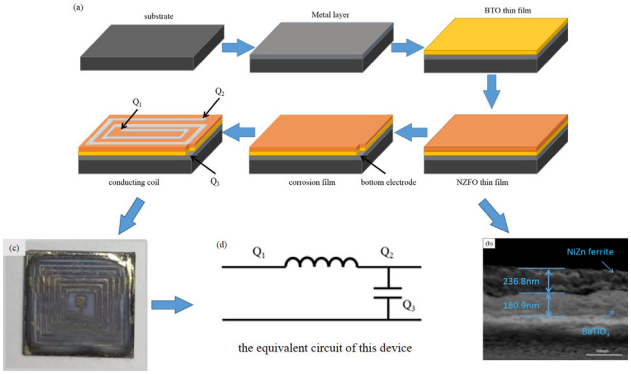

Figure 7 (a). The manufacturing process of the capacitance and inductance integrated device; (b). The SEM image of the cross-section drawn of composite thin film; (c). The photograph of the real device; (d). The equivalent circuit of the device

4. Conclusion

In this paper, BTO and NZFO films were successfully prepared by sol-gel method, and the effects of annealing temperature on the phase, surface morphology and properties of the films were investigated. The appropriate heat treatment temperature parameters were determined, and the BTO film and NZFO film with dielectric and ferromagnetism were prepared. On this basis, the two materials were combined to prepare a composite functional material film with both ferromagnetism and ferroelectricity. The capacitance and inductance integrated device was assembled, the result showed the device could increase the inductance by 20 %, and also had the capacitive characteristics.

Reference

[1] He X, Chen Y, Wang S, et al. Enhancing inductance of spiral copper inductor with BaFe12O19/poly (phenylene oxide) composite as an embedded magnetic core[J]. Composites Part B: Engineering, 2018, 138: 232-242.

[2] Anthony R , Wang N , Casey D P , et al. MEMS based fabrication of high - frequency integrated inductors on Ni-Cu-Zn ferrite substrates[J]. Journal of Magnetism & Magnetic Materials, 2016, 406: 89-94.

[3] Dai G, Zhang J. Concept and architecture technology of integrated microsystems [J]. Microelectronics, 2016, 46(1): 101-106.

[4] Chao S, Dogan F. BaTiO3–SrTiO3 layered dielec-

 DOI: https://doi.org/10.30564/ssid.v1i1.606

trics for energy storage[J]. Materials Letters, 2011, 65(6): 978-981.

[5] Khirade P P, Birajdar S D, Raut A V, et al. Multiferroic iron doped BaTiO3 nanoceramics synthesized by sol-gel auto combustion: influence of iron on physical properties[J]. Ceramics International, 2016, 42(10): 12441-12451.

[6] Choudhury A. Dielectric and piezoelectric properties of polyetherimide/BaTiO3 nanocomposites[J]. Materials Chemistry and Physics, 2010, 121(1-2): 280-285.

[7] Nayak S, Kumar Chaki T, Khastgir D. Development of poly (dimethylsiloxane) / BaTiO3 nanocomposites as dielectric material[C]. Advanced Materials Research. Trans Tech Publications, 2013, 622: 897-900.

[8] Dang Z M, Yu Y F, Xu H P, et al. Study on microstructure and dielectric property of the BaTiO3/ epoxy resin composites[J]. Composites Science and Technology, 2008, 68(1): 171-177.

[9] Dang Z M, Lin Y Q, Xu H P, et al. Fabrication and dielectric characterization of advanced BaTiO3/polyimide nanocomposite films with high thermal stability[J]. Advanced Functional Materials, 2008, 18(10): 1509-1517.

[10] Zhou T, Zha J W, Cui R Y, et al. Improving dielectric properties of BaTiO3/ ferroelectric polymer composites by employing surface hydroxylated BaTiO3 nanoparticles[J]. ACS applied materials & interfaces, 2011, 3(7): 2184-2188.

[11] Cernea M, Andronescu E, Radu R, et al. Sol–gel synthesis and characterization of BaTiO3-doped (Bi0.5Na0.5)TiO3 piezoelectric ceramics[J]. Journal ofAlloys and Compounds, 2010, 490(1-2): 690-694.

[12] Ashiri R, Nemati A, Ghamsari M S. Crack-Free nanostructured BaTiO3, thin films prepared by sol–gel dip-coating technique[J]. Ceramics International, 2014, 40(6): 8613-8619.

[13] Li J, Zhu G, Xu H, et al. Preparation, structure and dielectric properties of substrate-free BaTiO3, thin films by sol–gel method[J]. Journal of Materials Science Materials in Electronics, 2017, 28(17): 1-5.

[14] Whittam, J., Hector, A. L., Kavanagh, C., et al.Combination of solid state and electrochemical impedance spectroscopy to explore effects of porosity in sol-gel derived BaTiO3 thin films[J]. ACS Omega. 2018, 42(1): 20-22.

[15] Tripkovic D, Vukmirovic J, Bajac B, et al. Inkjet patterning of in situ, sol–gel derived barium titanate thin films[J]. Ceramics International, 2016, 42(1): 1840-1846.

[16] Suematsu K, Arimura M, Uchiyama N, et al. High-performance dielectric thin film nanocomposites of barium titanate and cyanoethyl pullulan: controlling the barium titanate nanoparticle size using a sol–gel method[J]. RSC Advances, 2016, 6(25): 20807-20813.

[17] ShinS H, Choi S Y, Lee M H, et al. High-performance piezoelectric nanogenerators via imprinted sol-gel BaTiO3 nanopillar array[J]. Acs Applied Materials & Interfaces, 2017, 9(47): 41099.

[18] Wang Y L, Wu W J, Mao W D, et al. Fast sintering soft ferrite materials at low temperature [J]. Journal of Inorganic Materials, 2003, 18(3): 601-605.

[19] Ghafoor A , Khan M A , Islam M U , et al. Structural and electromagnetic studies of Ni0.7Zn0.3Ho2x-Fe2−2xO4 ferrites[J]. Ceramics International, 2016, 42(12): 14252-14256.

[20] Gao J, Cui Y, Yang Z. The magnetic properties of NixZn1−xFe2O4, films fabricated by alternative sputtering technology[J]. Materials Science & Engineering B, 2004, 110(2): 111-114.

[21] Liu Y, Li Y, Zhang H, et al. Structural and magnetic properties of NiZn-ferrite thin films prepared by radio frequency magnetron sputtering[J]. Journal of Applied Physics, 2011, 109(7): 739.

[22] Zhong X, Phuoc N N, Soh W T, et al. Dynamic magnetization of NiZn ferrite doped FeSiAl thin films fabricated by oblique sputtering[J]. Journal of Magnetism & Magnetic Materials, 2017, 432: 373-381.

[23] Hashi S, Takada N, Nishimura K, et al. Fabrication technique for over 10-μm-thick ferrite particulate film at room temperature[J]. Magnetics IEEE Transactions on, 2005, 41(10): 3487-3489.

[24] Lee J J, Hong Y K, Bae S, et al. High-quality factor Ni-Zn ferrite planar inductor[J]. IEEE Transactions on Magnetics Mag, 2010, 46(6): 2417-2420.

[25] Li L, Peng L, Li Y, et al. Structure and magnetic properties of Co-substituted NiZn ferrite thin films synthesized by the sol–gel process[J]. Journal of Magnetism & Magnetic Materials, 2012, 324(1): 60-62.

[26] Gao P, Rebrov E V, Verhoeven T M W G M, et al. Structural investigations and magnetic properties of sol-gel Ni0.5Zn0.5Fe2O4 thin films for microwave heating[J]. Journal of Applied Physics, 2010, 107(4): 5223.

[27] Yusuf Y, Azis R S, Kanagesan S, et al. Microstructure and magnetic properties of Ni-Zn ferrite thin film synthesized using sol-gel and spin-coating technique[J]. Journal of the Australian Ceramic Society, 2017, 53(8): 1-8.

[28] Li B , Wang C , Liu W , et al. Synthesis of Co-doped barium strontium titanate nanofibers by sol–gel/electrospinning process[J]. Materials Letters, 2012, 75: 207-210.

DOI: https://doi.org/10.30564/ssid.v1i1.606